

THE DEVELOPMENT OF AN INJURY COST FUNCTION FOR CHILD PASSENGER SAFETY

Chris Sherwood, Rob Marshall, Jeff Crandall

University of Virginia

U.S.A.

Paper Number 07-0127

ABSTRACT

The design of the optimal child restraint environment must consider both vehicle system (VS) and child restraint system (CRS) components. The objective of this study was to analyze the contributions from each system using a computer simulation of a rear facing (RF) child restraint involved in frontal crash. A parametric study of the material characteristics of components in each system was performed, resulting in a total of 625 simulations. The results of each simulation were compared using a single Cost Function score based on head acceleration, neck tension, and chest acceleration values. This Cost Function was developed based on injury risk curves combined with monetary cost estimates of these injuries. The analysis found that the vehicle seat cushion, lower LATCH belt, and internal CRS cushion should be designed with higher stiffness values, while the internal harness should be made more compliant. Neck tension was the primary contributor to the total cost function.

INTRODUCTION

The automobile child restraint environment is a function of both the vehicle and the child restraint. To design the optimal child restraint environment, design parameters from both the vehicle system (VS) and child restraint system (CRS) must be considered. In addition, VS parameters must be designed with all occupant sizes and ages in mind, including both children and adults.

The goal of this project was to determine the VS and CRS parameters which have the greatest influence on child restraint safety performance in frontal crashes. A 12 month old child in a rear facing child restraint was studied, but in future work multiple occupant sizes would have to be considered simultaneously.

First, a technique was developed to evaluate the risk of injury to a child based on measured forces and accelerations, which could be recorded during sled tests or computer simulations of sled tests. Multiple outcome measures are available when testing child restraint systems. A cost function must be developed

that provides an objective method for combining multiple measurements into a single comparative value. Injury risk curves and estimates of the monetary cost of these injuries were combined to develop an overall injury cost based on the most critical body regions.

Second, a computational model of a 12 month old child in a rear facing child restraint, in a frontal crash, was developed. The model was validated against a sled test.

Finally, the computational model was used to assess the importance of VS and CRS parameters in this model. A parametric study varying the material properties of the vehicle seat cushion, lower LATCH belt, child restraint harness, and child restraint cushion was performed with a total of 625 simulations. The cost function developed earlier was used to rate the relative risks of the variable combinations.

METHODS

Injury Cost Function

The purpose of the Total Cost Function is to quantify the overall cost of injury to the dummy in a given loading condition. The dummy has a large number of injury measures which could be incorporated into the Cost Function. Other output parameters of the system, such as rotation angle or excursion distances, could also be used but quantification of the cost associated with these parameters is difficult. Therefore, the final Cost Function only uses injury measures from the head, neck, and chest body regions.

$$\text{Total Cost} = \text{Cost}_{\text{Head}} + \text{Cost}_{\text{Neck}} + \text{Cost}_{\text{Chest}} \quad [1]$$

One of the criteria used to certify rear facing child restraints in FMVSS 213 (NHTSA, 2003) is the Head Injury Criteria (HIC_{36}), and this calculated measure was also chosen to best represent the risk of head injury in the Cost Function. The maximum value allowed for HIC_{36} in the FMVSS 213 standard is 1000.

In addition to the HIC_{36} limit, the other injury requirement in dynamic tests of rear facing child

restraints for FMVSS 213 standards is chest acceleration (3ms clip, measured on the spine at the equivalent position of T1), with an allowed peak value of 60 g's. This injury measure was chosen to best represent the risk of injury to the bony thorax, thoracic organs, and abdominal organs.

The neck is also a body region of critical importance for young children. The primary reason for restraining young children in rear facing child restraints is to protect the neck. For adults the neck injury criterion (N_{ij}) is commonly used to assess neck injury risk. The N_{ij} calculation is a combined injury criteria for the upper neck which incorporates both axial forces and sagittal bending moments. There are questions, however, about the biofidelity of the neck in the CRABI 12 month dummies. The CRABI 12 month dummy can measure high extension moments despite limited amounts of actual upper neck bending in a rear facing child restraint (Sherwood et al., 2004). It is hypothesized that the design of the neck, which does not include an atlanto-occipital joint at the neck/head interface, may account for some of these high values. For these reasons, the cost function includes peak Upper Neck Tension rather than N_{ij} as the injury measure to quantify neck injury risk.

The Total Cost Function did not include any kinematic measurement due to the difficulty in relating the rotation angle to a quantifiable injury risk and associated cost. The FMVSS 213 standard does, however, include a limit on the child restraint angle (70°, measured at the dummy's back with respect to vertical). This limit is included as a constraint in the simulations, excluding any simulations if this 70° limit is exceeded.

The next step was to relate each injury measure to a probability of injury risk at different AIS levels. An example of this procedure is shown graphically in Figure 1, using sample HIC injury probability curves. For a given injury measure, the probability of an AIS 1 injury was calculated by subtracting the probability of an AIS 2+ injury from the probability of an AIS 1+ injury ($0.9 - 0.57 = 0.33$) (Kuchar et al., 2001). This technique provides probability values of receiving each AIS level of injury, and these probabilities sum to 1.

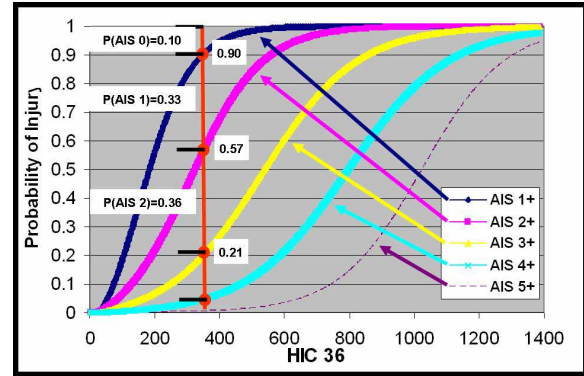


Figure 1. Graph of the method for determining the probability of injury for different AIS levels (data shown for illustrative purposes only).

The probability of injury equations for each injury measure are included in Equations 2-4. The HIC36 curves were scaled from data for the 50th percentile male using a scale factor of 0.5, and the neck tension curves were scaled from data for the 3 year old child using a scaling factor of 0.9 (Eppinger et al., 1999). The chest acceleration curves were scaled from data for the 50th percentile male using a scale factor of 0.833 (Eppinger et al., 1999).

$$\begin{aligned}
 &\text{Head Injury Risk} \\
 P(\text{AIS} \geq 1) &= \text{CND}, \ln(\text{HIC}_{36}/0.5), \text{ Mean} = 5.356, \text{ SD} = 1.009 \\
 P(\text{AIS} \geq 2) &= \text{CND}, \ln(\text{HIC}_{36}/0.5), \text{ Mean} = 6.964, \text{ SD} = 0.847 \\
 P(\text{AIS} \geq 3) &= \text{CND}, \ln(\text{HIC}_{36}/0.5), \text{ Mean} = 7.452, \text{ SD} = 0.740 \\
 P(\text{AIS} \geq 4) &= \text{CND}, \ln(\text{HIC}_{36}/0.5), \text{ Mean} = 7.656, \text{ SD} = 0.607 \\
 P(\text{AIS} \geq 5) &= \text{CND}, \ln(\text{HIC}_{36}/0.5), \text{ Mean} = 7.696, \text{ SD} = 0.587
 \end{aligned} \tag{2}$$

$$\begin{aligned}
 &\text{Neck Injury Risk} \\
 P(\text{AIS} \geq 1) &= (1 + \text{EXP}(-(-3.272 + 0.00268 * Fz/0.9))) - 1 \\
 P(\text{AIS} \geq 2) &= (1 + \text{EXP}(-(-3.454 + 0.00268 * Fz/0.9))) - 1 \\
 P(\text{AIS} \geq 3) &= (1 + \text{EXP}(-(-3.655 + 0.00268 * Fz/0.9))) - 1 \\
 P(\text{AIS} \geq 4) &= (1 + \text{EXP}(-(-4.422 + 0.00268 * Fz/0.9))) - 1 \\
 P(\text{AIS} \geq 5) &= (1 + \text{EXP}(-(-5.956 + 0.00268 * Fz/0.9))) - 1
 \end{aligned} \tag{3}$$

$$\begin{aligned}
 &\text{Chest Injury Risk} \\
 P(\text{AIS} \geq 2) &= (1 + e^{(1.232 - 0.0576 * (\text{Chest}_{3ms}/0.833))}) - 1 \\
 P(\text{AIS} \geq 3) &= (1 + e^{(3.149 - 0.063 * (\text{Chest}_{3ms}/0.833))}) - 1 \\
 P(\text{AIS} \geq 4) &= (1 + e^{(4.343 - 0.063 * (\text{Chest}_{3ms}/0.833))}) - 1 \\
 P(\text{AIS} \geq 5) &= (1 + e^{(8.765 - 0.0659 * (\text{Chest}_{3ms}/0.833))}) - 1
 \end{aligned} \tag{4}$$

where,
CND = Cumulative Normal Distribution
ln = Natural Log
SD = Standard Deviation

The next step was to quantify the “cost” of each level of AIS injury. This was accomplished by using estimates on actual costs (medical, insurance, etc.) using HARM 2000 data (Miller et al., 2001). These estimates were assumed to be valid for children, although the paper was based on adult data. The HARM 2000 data is based on MAIS injury levels at one body region, while the costs for multiple body regions cannot be summed to provide precise estimates of whole-body injury costs. The purpose of this Cost Function procedure is not to provide

accurate monetary cost estimates, but rather to quantify total injury risk in a comparative analysis. The HARM cost estimates are used as scaling factors to compare between AIS injury levels (relating an AIS 2 head injury to an AIS 3 head injury) and between body regions (relating an AIS 2 head injury to an AIS 2 neck injury). To make the HARM estimates dimensionless, each cost estimate was divided by the largest singular cost estimate (\$1,617,797 – MAIS 5 Spinal Cord). Table 1 shows the Total Monetary Costs and Scaled Costs, not including Quality of Life adjustments, which were taken from this study using MAIS injury levels for the Brain (HIC₃₆), Spinal Cord (Neck Tension), and Trunk and Abdomen (Chest Acceleration 3ms clip).

Table 1. Harm 2000 Total Monetary Costs and the equivalent dimensionless scaled costs

Body Region	MAIS	Total Monetary Costs	Scaled Costs
Brain	1	\$57,858	0.036
	2	\$59,911	0.037
	3	\$233,250	0.144
	4	\$377,577	0.233
	5	\$1,058,295	0.654
Spinal Cord	3	\$818,588	0.506
	4	\$1,366,923	0.845
	5	\$1,617,797	1.000
Trunk and Abdomen	1	\$8,645	0.005
	2	\$58,168	0.036
	3	\$89,911	0.056
	4	\$153,604	0.095
	5	\$198,760	0.123

The cost for each body region was calculated by multiplying the probability of injury at each AIS level with the Scaled Cost value at the corresponding AIS level (Equations 5-7).

$$\text{Cost}_{\text{Head}} = \sum_{\text{Head}} (\text{Risk AIS 1}) \cdot (\text{Scaled HARM AIS 1}) + (\text{Risk AIS 2}) \cdot (\text{Scaled HARM AIS 2}) + (\text{Risk AIS 3}) \cdot (\text{Scaled HARM AIS 3}) + (\text{Risk AIS 4}) \cdot (\text{Scaled HARM AIS 4}) + (\text{Risk AIS 5}) \cdot (\text{Scaled HARM AIS 5}) \quad [5]$$

$$\text{Cost}_{\text{Neck}} = \sum_{\text{Neck}} (\text{Risk AIS 3}) \cdot (\text{Scaled HARM AIS 3}) + (\text{Risk AIS 4}) \cdot (\text{Scaled HARM AIS 4}) + (\text{Risk AIS 5}) \cdot (\text{Scaled HARM AIS 5}) \quad [6]$$

$$\text{Cost}_{\text{Chest}} = \sum_{\text{Chest}} (\text{Risk AIS 1}) \cdot (\text{Scaled HARM AIS 1}) + (\text{Risk AIS 2}) \cdot (\text{Scaled HARM AIS 2}) + (\text{Risk AIS 3}) \cdot (\text{Scaled HARM AIS 3}) + (\text{Risk AIS 4}) \cdot (\text{Scaled HARM AIS 4}) + (\text{Risk AIS 5}) \cdot (\text{Scaled HARM AIS 5}) \quad [7]$$

For the purpose of having a more efficient way to calculate the cost for each body region without using normal distribution tables, each of the three components of the total cost function was estimated with a polynomial equation determined by a polynomial curve fitting routine. Both the risk curves for each AIS injury level and the scaled HARM costs were incorporated into these functions (Equations 8-10). The curves were fit with an 8th order polynomial function in each case.

$$\text{Cost}_{\text{Head}} = -2.824\text{E-}3 + 2.972\text{E-}4 \cdot \text{HIC}_{36} - 1.403\text{E-}6 \cdot \text{HIC}_{36}^2 + 4.787\text{E-}9 \cdot \text{HIC}_{36}^3 - 6.490\text{E-}12 \cdot \text{HIC}_{36}^4 + 4.628\text{E-}15 \cdot \text{HIC}_{36}^5 - 1.853\text{E-}18 \cdot \text{HIC}_{36}^6 + 3.953\text{E-}22 \cdot \text{HIC}_{36}^7 - 3.503\text{E-}26 \cdot \text{HIC}_{36}^8 \quad [8]$$

$$\text{Cost}_{\text{Neck}} = 1.765\text{E-}2 - 4.174\text{E-}5 \cdot \text{NeckF}_z + 7.674\text{E-}7 \cdot \text{NeckF}_z^2 - 1.937\text{E-}9 \cdot \text{NeckF}_z^3 + 2.842\text{E-}12 \cdot \text{NeckF}_z^4 - 2.017\text{E-}15 \cdot \text{NeckF}_z^5 + 7.375\text{E-}19 \cdot \text{NeckF}_z^6 - 1.360\text{E-}22 \cdot \text{NeckF}_z^7 + 1.006\text{E-}26 \cdot \text{NeckF}_z^8 \quad [9]$$

$$\text{Cost}_{\text{Chest}} = 9.468\text{E-}3 + 4.371\text{E-}4 \cdot \text{Chest}_{3\text{ms}} + 8.219\text{E-}6 \cdot \text{Chest}_{3\text{ms}}^2 + 1.243\text{E-}7 \cdot \text{Chest}_{3\text{ms}}^3 - 8.731\text{E-}9 \cdot \text{Chest}_{3\text{ms}}^4 + 2.213\text{E-}10 \cdot \text{Chest}_{3\text{ms}}^5 - 2.877\text{E-}12 \cdot \text{Chest}_{3\text{ms}}^6 + 1.796\text{E-}14 \cdot \text{Chest}_{3\text{ms}}^7 - 4.265\text{E-}17 \cdot \text{Chest}_{3\text{ms}}^8 \quad [10]$$

Computational Model

The computational model was developed based upon a sled test using the Safety 1st Comfort Ride (Model # 22-400-GRC) child restraint in the rear facing orientation with a CRABI 12 month dummy. The child restraint was attached to a 2001 Ford Windstar bench seat using a lower LATCH belt and a foam spacer. The sled test simulated an FMVSS 213 child restraint test, with a velocity of approximately 48 km/hr (30 mph).

The model simulation was performed in the multibody simulation environment MADYMO 6.1. All model components are rigid bodies with defined mass and inertia. Either ellipsoids or finite element meshes were used to describe the component geometry. While some simplifications are inherent in this modeling technique, the models are computationally efficient and can reasonably simulate global responses to various impacts.

The third row bench seat of a Ford Windstar was modeled as two rigid finite element surfaces with dimensions approximating the actual seat (Figure 3). The interaction between the child restraint and the vehicle seat cushion was modeled with a prescribed force versus deformation relationship. The geometry

of the Safety 1st child restraint was obtained from a 3D measurement of characteristic points on the seat, which were converted into a rigid finite element mesh. This model is also defined as one rigid body.

The child restraint was attached to the vehicle with a lower LATCH belt and a body represented by the foam “noodle” used in the sled test. In many rear facing child restraints a foam noodle or other object must be placed under the base of the child restraint to provide the correct child restraint angle. Without the noodle, the child restraint would be too upright. Since the noodle has minimal initial deformation is no longer under load as the child restraint moves forward during the crash pulse, it was included as a rigid body. The lower LATCH was attached from the LATCH anchorages to fixed points on the child restraint, and was modeled as a multibody belt segment with a non-linear elastic characteristic. The initial pre-tension of the belt was approximately 200 N.

The internal harness is constructed of two shoulder belts which span from above the shoulders to a buckle near the pelvis, two lap belts which span from outside of the thigh to the center buckle, and a single belt which joins the center buckle to the child restraint between the thighs. The belt for the five point restraint is modeled as a multibody element. A multibody belt system consists of a chain of non-linear elastic spring segments. The belt model allows slip between two adjacent belt segments through slings. The slip depends on a friction coefficient. At each belt slip ring, a different friction coefficient can be defined to control the slip of belt material between the two adjacent belt segments. Thus no contact models are defined between dummy and belts, but a kinematic constraint is applied at predefined points on the dummy and the child restraint. The harness clip and buckle are modeled as ellipsoid rigid bodies because they do contact the dummy.

A child occupant was modeled using the CRABI 12 month old child dummy model. It is scaled down from the Hybrid III 50th percentile male dummy model. The MADYMO manual reports the dummy to be completely similar in structure to the 50th percentile model. The dummy is a global ellipsoid model that is computationally efficient and can simulate global responses to various impacts.

The positioning of the dummy is executed by simultaneously applying a gravitational force on the seat and dummy while they are positioned right

above the backseat of the car. In order to achieve the required initial stiffness on the lower LATCH belt, a separate pre-tensioning system is modeled. These systems are modeled just to apply the required initial force to the belts which occurs during installation. Once the correct amount of tension is applied during the pre-simulation, the belt lengths are locked so that each belt will behave only according to its stiffness characteristics. This pre-simulation is run until an equilibrium state is achieved for dummy and child restraint.

Results for the child seat kinematics are shown in Figure 2, and selected dummy injury measures are included Table 2. Images of the sled test and simulation at several time intervals are shown in Figures 2 and 3. The kinematics between the sled test and model are very similar for both the child restraint and dummy. The angle of the child restraint in the simulation is within 3 degrees of the sled test at all times until approximately 75 ms, at which point all injury values have reached their maxima. At this time, the child restraint in the sled test continues to rotate, but it appears to be partially due to sliding on the vehicle seat, and this movement is not captured in the model.

Table 2. Selected output measures for the sled test and simulation

Injury and Kinematic Measures	Units	Sled Test	Simulation	Percent difference
HIC15		279	221	21%
HIC36		436	340	22%
Head Res Acc, 3ms clip	g's	55.9	48.8	13%
Chest Res Acc, 3ms clip	g's	30.6	44.6	46%
Pelvis Res Acc, 3ms clip	g's	52.5	46.3	12%
Upper Neck Tension	N	1183	973	18%
Rearward rot. Angle @ 55 ms	Deg	8.1	8.8	9%



Figure 2. Sled test images at 0, 30, 60, and 90 ms.

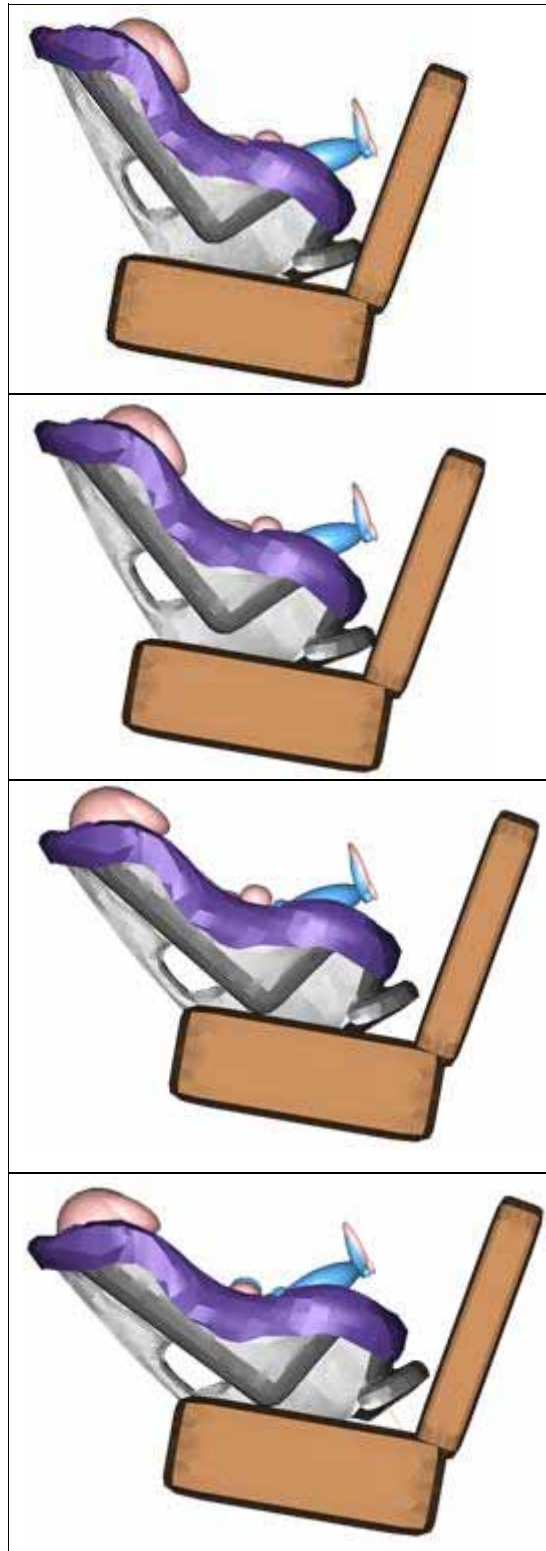


Figure 3. Simulation images at 0, 30, 60, and 90 ms.

The injury values in Table 2 are all within 22% of the sled test values, with the exception of the chest acceleration which was 46% higher in the simulation. In the sled test, the head had a much higher resultant acceleration than the chest (56 g's vs. 30.6 g's). The head and chest values were much closer in the simulation (48.8 vs. 44.6). Because the most common and serious injuries to children are head injuries, more weight was given to the head accelerations when validating the model.

One possibility for the difference between the simulation and the sled test was the deformation of the child restraint shell. The child restraint is designed with stiffening components on the back of the child restraint, but the majority of these do not extend to the portion of the child restraint where the dummy's head is located. The video of the sled test shows that the upper portion of the child restraint flexes, however the effect on the head acceleration is unknown.

Parametric Study

The validated computational model was used in the parametric study with MADYMO 6.2 and MADYMO/AutoDOE 2.3 to set up and run the simulations with the modified variables. The variables used were the Vehicle Cushion Stiffness, LATCH Belt Stiffness, CRS Harness Stiffness, and CRS Cushion Stiffness. The Vehicle and CRS cushion stiffness are defined as functions of Force vs. Displacement. The LATCH Belt and CRS Harness stiffness are defined as functions of Force vs. Strain. The stiffness values were parameterized by scaling the Force values of these functions.

Each variable was evaluated at 5 levels, from 5 times to 1/5th its original value. The variables were distributed logarithmically so the 5 levels were 0.2, 0.44721, 1.0, 2.236 and 5.0. A full factorial design of experiments was used evaluating all of the combinations of the variables. This resulted in a total of 625 simulations. The simulations were run using approximately 1 week of CPU time.

Input and output variables were plotted and compared to each other. When an input variable was plotted against an output variable, average values of all the simulations using that variable level were determined and plotted with lines connecting these average values. When two different output variables were plotted against each other a least squares fit of a straight line was determined and plotted to show a linear trend. It should be noted, however, that trends in the average values include all case simulations,

and that these quantities may not reflect the same information when looking for best case scenarios.

The cost variables (head injury cost, neck injury cost, chest injury cost, and total injury cost,) were all divided by the total injury cost of the baseline model (all variables at level 1.) This was done to show the relative change from the baseline cost. These cost values should not be directly compared to injury costs in previous sections of this paper.

RESULTS

The 625 simulations ran to completion with no errors. Visual inspection of the kinematics of each simulation was not done. The minimum, average, and maximum values of the output variables of all 625 simulations are shown in Tables 3-6 below. One simulation exceeded the FMVSS 213 limit of 70 degrees maximum seat back angle. All simulations met the HIC 1000 limit, and most of the simulations fell below the Chest 3ms limit of 60g's.

Table 3. Normalized injury costs for all simulations.

Normalized Cost	Minimum	Average	Maximum
Total	0.316	0.974	3.389
Head	0.071	0.145	0.582
Chest	0.089	0.125	0.215
Neck	0.110	0.705	2.771

Table 4. Relative percentage of injury cost by body region.

Percentage of Normalized Total Cost	Minimum	Average	Maximum
Head	3.4%	15.7%	37.0%
Chest	4.6%	17.7%	39.2%
Neck	32.6%	66.6%	89.5%

Table 5. Injury criteria for all simulations

	Minimum	Average	Maximum
Chest 3ms (g's)	30.3	42.7	72.7
HIC 36	154	299	710
HIC 15	98	207	710
Peak Neck Tens (N)	272	926	2439

Table 6. CRS motion for all simulations

	Minimum	Avg	Maximum
Seat Back Angle (deg)	45	55.1	70.2
Forward Excurs (mm)	690	760	846

Figure 4 shows the Normalized Total Cost of each simulation sorted by rank. The head, neck, and chest cost components of each simulation are also plotted. The total cost was dominated by the neck cost.

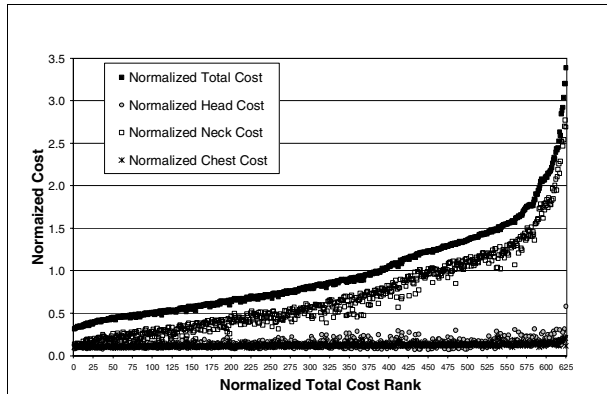


Figure 4. Normalized costs for all simulations.

Figure 5 shows the effect of Vehicle Cushion Stiffness on the Total Cost. The average total cost decreased with both more compliant and stiffer vehicle cushions, although the simulations with the lowest total costs had the stiffest seats. Neck tension had the largest decrease with increasing vehicle cushion stiffness. Chest accelerations tended to increase with increasing vehicle cushion stiffness, while HIC values followed the total cost trend with the baseline value resulting in the highest HIC scores.

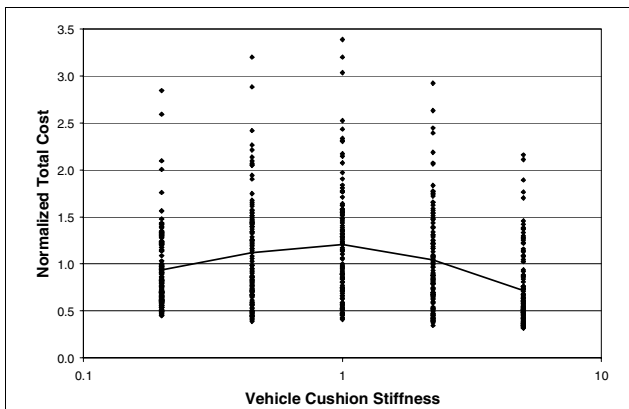


Figure 5. Total cost vs. vehicle cushion stiffness values.

Figure 6 shows the effect of LATCH belt stiffness on injury cost. The average values of total cost, neck tension, Chest G's and HIC all decrease with a more compliant LATCH belt, and increase with a stiffer LATCH belt. The simulations with the lowest total costs and the lowest injury measures occur at all LATCH stiffness levels, however.

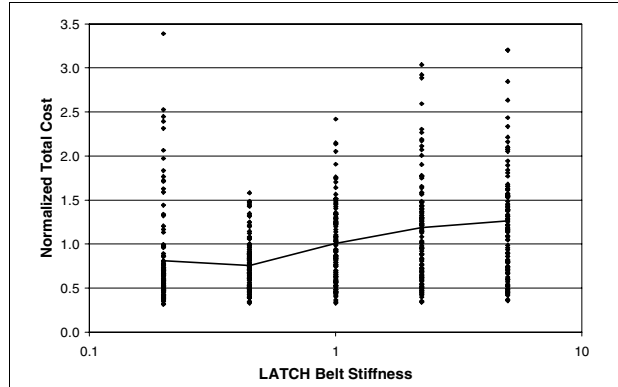


Figure 6. Total cost vs. LATCH belt stiffness values.

A more compliant CRS cushion increases the average values of total cost (Figure 7), neck tension, HIC, and Chest G's. The more compliant cushion allows a differential velocity to develop between the occupant and the CRS. This is similar to having slack in the seat belt of an adult occupant in a frontal collision. This situation should be minimized by having a stiffer CRS cushion.

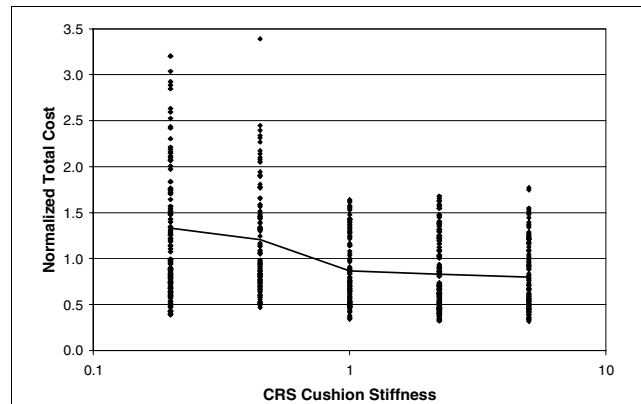


Figure 7. Total cost vs. CRS cushion stiffness values.

A more compliant CRS Harness reduces total cost (Figure 8), neck tension, Chest G's and HIC, although the effect on reducing HIC is minimal. As the occupant moves vertically in the CRS due to its reclined angle, the CRS Harness acts as a spring that couples the occupant to the CRS and ultimately to the vehicle structure. A less stiff spring reduces the applied force on the occupant, but may allow more excursion of the child. This possibility was not analyzed in this study. The effect on HIC is minimal which suggests that HIC is more sensitive to the contact between the head and the CRS, as opposed to the restraining forces applied by the harness.

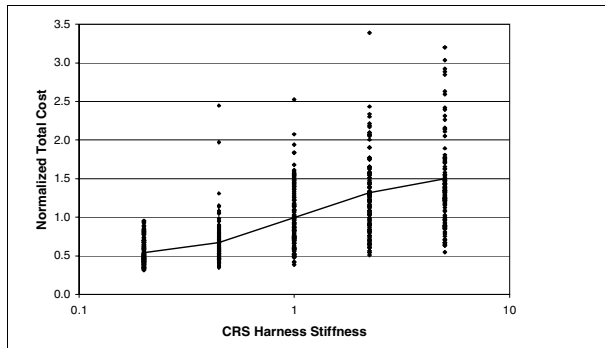


Figure 8. Total cost vs. CRS harness stiffness values.

LIMITATIONS

This parametric study is by no means an accurate reflection of the true vehicle fleet or the different CRS models that are available. The results are used to investigate trends in configurations similar to that of the Safety 1st CRS in a FMVSS 213 condition on a Windstar seat.

The model does not have the detail to show how the CRS interacts with either the metal structure under the vehicle seat cushion, or how the CRS might roll off the front of the seat cushion when it translates too far forward.

The range of the variables chosen for the parametric study was arbitrary. More importantly, it is not known if the range of variation in the vehicle seat cushion underestimates or overestimates the range in the actual vehicle fleet. The outputs are shown to be sensitive to the vehicle cushion based on the ranges chosen. It would be important to know how this relates to the true vehicle fleet.

Seat geometry was also not varied in this study, and a simplified vehicle cushion stiffness model was used. This lumps all of the parameters such as foam stiffness, underlying structure, and overall geometry into one function. Different seat designs may show different results.

The LATCH belt stiffness was varied in this analysis. The LATCH belt was modeled as a line and did not translate with respect to the child restraint. This technique may not capture the more complex interaction as the belt passes through openings in the CRS and slides inside the CRS slot. Therefore the variable of LATCH belt stiffness may actually describe the entire system of attachment between the CRS and the LATCH belt.

Different fixation methods of the CRS were also not explored. Tether systems and other types of fixation may dramatically change the motion of the CRS relative to the vehicle. In addition, the interaction of the child restraint with other vehicle structures (front vehicle seat, front dash) was not included. This interaction and its relationship with excursion is likely a critical factor and must be considered in future research.

All of these assumptions and simplifications should be taken into consideration when evaluating the results of the simulations. Additional sled tests should be used to further test the hypotheses put forth by this parametric analysis.

DISCUSSION

Neck injury is the largest component of the cost function in most of the cases explored in the simulations. The parameter values which were most beneficial were those that limited the neck tension peak value. This differs from research which shows that the most commonly injured body region is the head (Arbogast, 2005). Real world data of child injuries, or child cadaveric research, are needed to further analyze the validity of the cost function, specifically ranking the relative importance of the different injury measures.

Although not addressed specifically in this report, contact with other vehicle structures has the potential to increase the injury risk of rear facing child restraints. The model used for this analysis did not include other interior vehicle structures, and thus judgments about excursion amounts were made without specific data. If, however, it can be assumed that excursion distances should be limited, the following conclusions were made; Vehicle Cushion Stiffness, LATCH Belt Stiffness, and CRS Cushion Stiffness values should all be increased, while the CRS Harness should be made more compliant.

The variable that had the greatest effect on injury cost and neck tension was the CRS harness stiffness. As the occupant moves up the CRS seat back during the crash event, it is restrained by the CRS harness. The stiffness of the CRS harness provides an opportunity for energy absorption by allowing more excursion of the dummy, which results in lower neck tension values. The CRS tested was a convertible CRS which allows for both rear facing and forward facing configurations. The harness may be designed for the forward facing case, resulting in a stiffness that should be reduced to optimize the benefit in the rear facing orientation.

CONCLUSIONS

One of the goals of this project was to develop a procedure for optimizing design variables from both the Vehicle System and Child Restraint System simultaneously, in order to minimize the injury risk to child occupants. This procedure was performed using a one year old dummy in a rear facing child restraint as an initial step in researching this process. A more in-depth, long term research project is required, however, to apply this procedure to the entire spectrum of occupant and restraint combinations. For example, there is little value in optimizing the restraint environment for a 12 month old in a rear facing child restraint without considering the effects on a 6 year old in a booster seat or an adult occupant. Future research on this topic should address the following topics:

- 1) all occupant ages and sizes
- 2) all restraint systems (vehicle belt, child restraints)
- 3) methods for improving the cost function validity by considering real world injury trends
- 4) realistic models of vehicle seats, including accounting for fleet variations
- 5) realistic ranges of system design parameters (Vehicle and Child Restraint)
- 6) child restraint fixation methods not currently used
- 7) the importance of excursion distances and occupant/child restraint contact with other vehicle structures
- 8) validation of findings with physical testing

ACKNOWLEDGEMENTS

This work was funded by the National Highway Traffic Safety Administration Contract DTRS 57-03-D-30005. The views expressed are those of the authors and not necessarily those of NHTSA.

REFERENCES

Arbogast, K., Jermakian, J., Ghati, Y., Smith, R., Maltese, M., Menon, R. (2005) Predictors and Patterns of Pediatric Head Injury in Motor Vehicle Crashes. Proc. 2005 IRCOBI Conference.

Eppinger, R., Sun, E., Bandak, F., Haffner, M., Khaewpong, N., Maltese, M., Kuppa, S., Nguyen, T., Takhounts, E., Tannous, R., Zhang, A. Development

of Improved Injury Criteria for the Assessment of Advanced Automotive Restraint Systems – II. National Highway Traffic Safety Administration. November, 1999.

Kuchar, A., Neat, G., Greif, R. (2001) A Systems Modeling Methodology for Evaluation of Vehicle Aggressivity in the Automotive Accident Environment, Paper 2001-01-1172, Society of Automotive Engineers, Warrendale, Pennsylvania.

Miller, T., Romano, E., Zaloshnja, E., Spicer, R. (2001) HARM 2000: Crash Cost and Consequence Data for the New Millennium, Proc. 45th AAAM, pp. 159-184.

National Highway Traffic Safety Administration (2003). "Federal Motor Vehicle Safety Standards: Child Restraint Systems." Federal Register 67(84): 21836-21852.

Sherwood, C, Abdelilah, Y, Crandall, J, Stevens, S, Saggese, J, Eichelberger, M. (2004) The Performance of Various Rear Facing Child Restraint Systems in a Frontal Crash. Proc. 48th AAAM.